Received: 4 May 2019 | Revised: 10 November 2019 | Accepted: 2 December 2019

DOI: 10.1002/ese3.671

Energy Science & Engineering
Open Access

RESEARCH ARTICLE

Longitudinal interference analysis of shale gas multi-stage fracturing horizontal wells upon high-precision pressure test

Dapeng Gao[1,2] | **Yuewu Liu**[1,2] | **Songqi Pan**[3,4] | **Jue Wang**[4] | **Xinmao Zhou**[4]

[1]Institute of Mechanics, Chinese Academy of Sciences, Beijing, China

[2]University of Chinese Academy of Sciences, Beijing, China

[3]Helmholtz Centre Postdam German Research Centre for Geosciences, Potsdam, Germany

[4]PetroChina Research Institute of Petroleum Exploration & Development, Beijing, China

Correspondence
Yuewu Liu, Institute of Mechanics, Chinese Academy of Sciences, Beijing 100190, China.
Email: lywu@imech.ac.cn

Funding information
PetroChina Innovation Foundation, Grant/Award Number: 2017D-5007-0208; Southwest Petroleum University, Grant/Award Number: PLN201711; National Natural Science Foundation of China, Grant/Award Number: 11702300

Abstract

Shale gas plays a crucial role in the national energy supply. However, fast pressure drop, production decline, and water resources pollution caused by well interference and fracture hits become more severe in multi-layer mining shale gas fields. Such as, it is urgent to evaluate the interference of multi-stage fracturing horizontal wells (MFHWs) between the upper and lower gas layers in Chinese Jiaoshiba shale gas field. Therefore, we put forward a comprehensive method to analyze the MFHW interference in this paper. The method contains bottom-hole pressure response analysis (BHPRA) during neighboring well fracturing, BHPRA of well interference test, and production dynamic analysis. Our study indicates that longitudinal pressure interference exists between the Jiaoshiba upper and lower gas layers upon the apparent interference pressure response in a multi-well test. However, MFHW interferences occur in the corresponding fracturing stages with shorter distance, and the interference strength is related to both well distance and fracturing scales. The Jiaoshiba upper gas layers can be developed to increase the gas production performance, but it is necessary to maintain a reasonable well spacing to avoid severe interference during the development.

KEYWORDS

industrial application, industrial engineering, multi-stage fracturing horizontal wells, numerical analysis, pressure response analysis, shale gas, well interference

1 | INTRODUCTION

Shale gas is a relatively clean fossil energy, and the development of the natural gas resources may lead to energy independence in some countries. Multi-stage fracturing horizontal well (MFHW) is a crucial technology of shale gas development, and the large-scale horizontal well pattern has achieved remarkable performance in many fields in North America and China.[1-5] However, some MFHW groups have appeared increasingly severe well interference after producing for several years, due to the well pattern infilling and large-scale hydraulic fracturing of new wells. For instance, Jiaoshiba is the most successful shale gas reservoir with more than 10 billion cubic meters cumulative gas production in China. Unfortunately, parent wells crop up jumps in water production during hydraulic fracturing processing of child wells in the later production period. Besides, North American shale fields, such as Arkoma Basin, have also shown an obvious loss of gas production because of well interference.[6,7] Fracture hits and pressure interference are two main factors influencing the shale gas permanent development.[8] The future high production

performance and stable production have been greatly challenged. Large-scale hydraulic fracturing has environmental risks for surface water and groundwater, especially contaminants may be transported by fracturing-induced fractures and natural fractures. The water environment problems caused by shale gas development have been highly valued by many countries.[9] Understanding the migration of the injected fracturing fluid is of great significance for determining whether the groundwater pollution in the reservoir is hidden.

Well interference may be caused by interaction between primary hydraulic fractures (HFs) and/or secondary natural fractures activated during hydraulic fracturing. Well interference analysis can help to understand the reasonable well spacing, increase the production of single well shale gas, save costs, and reduce the amount of fracturing fluid and the treatment and discharge of return fluid. The development of the 300-m well spacing in the lower layers in Jiaoshiba shale gas field obtain satisfied gas production performance. However, will the development of new MFHWs in the upper layers affect the production of the old wells in the lower gas reservoir? The shale gas reservoir has a tremendous difference in the horizontal and vertical permeability, and the permeability in the longitudinal direction is relatively low. Does the longitudinal well interference exist? Well interference may cause gas productivity to drop (occasionally rise) because of changing existing fracture networks, near-well permeability, or due to multiphase flow. This process is called fracture hit, and three different mechanisms are thought to cause well interference: depleted zones, changes in the geo-stress field, and high-permeability lithofacies. In particular, the well interference in the longitudinal direction needs to be recognized, and it is necessary to pay special attention to whether the fracturing fluid will reach the upper horizon and whether the fracturing fluid may enter the upper layer to affect the groundwater system.

Conventional well interference evaluation methods include static and dynamic analysis methods. Static analysis methods mainly include log curve comparison and well reservoir parameter comparison. Dynamic analysis methods mainly include interference test, tracer test, interwell microseismic, and geochemical methods. Among them, the interference test well belongs to the multi-well test well, which can obtain the reservoir information of a region, including directly detecting whether the wells are connected, whether the interwell fault is closed, the dominant seepage channel of the stratum, and the trend of the fracture. The interference well test usually includes one active well and multiple observation wells. During the test, the observation wells are always kept closed, and the pressure and background pressure measured by the observation wells are compared to explain the formation parameters and pressure diffusion of the high-permeability reservoir channel. Classical interference testing techniques are based on the superposition of the line source solution. The use of this method is limited by the precision and time resolution that is normally obtained when measuring the production rate in active wells. In the high-precision pressure test technique proposed by Najurieta et al,[10] the pressure signal is measured at the active well and it is used to accurately calculate its diffusion in the reservoir. The higher precision in pressure calculation at the observing well gives more resolution to the analyst and provides more confidence when evaluating local reservoir heterogeneities.

To recognize the well interference and analyze its impact on production, many scholars have presented some new methods in recent years. These methods can be divided into three types: (a) to investigate the well interference by fine-scale reservoir numerical modeling; (b) calculate the interference extent by statistic the pressure/production disturbance caused by fracture hit; and (c) using pressure transient analysis to recognize the well interference.

1. Fine-scale reservoir numerical modeling. Mezghani et al[11] combined gradual deformation and upscaling techniques for direct conditioning of fine-scale reservoir models to interference test data, as a consequence, both fine- and coarse-scale models are updated by dynamic data during the history matching process, and they used a synthetic interference test to validate the proposed methodology. Marongiu-Porcu et al[12] proposed a numerical simulation method for shale gas reservoirs based on geophysical, completion and development data of Eagle Ford shale gas fields and studied the propagation of HFs and their respective network with natural fractures. The magnitude and orientation of in situ stress were evaluated.
2. Statistic method to analyze the pressure/production disturbance caused by fracture hit or well interference. Sardinha et al[8] counted 763 pressure disturbances detected by neighboring wells in 252 fracture events in a well group of 10 wells in the Nexen Dilly Greek shale gas field and analyzed the number of pressure fluctuations, amplitude, and well spacing and horizon layer relationship. Yaich et al[13] presented a new statistic method to quantify the impact of well interference and optimize well spacing in the Marcellus Shale. Pang et al[14] studied the effect of well interference on shale gas well stimulated reservoir volume (SRV) interpretation. Liang et al[15] share their monitoring data addressing well connectivity and fracture hit mitigation through an integrated modeling approach on multi-pad development. Molina and Zeidouni[16] presented a calculation method of well interference strength, which is considered to be the number of stages connected to the fracturing stage.
3. Pressure transient analysis to recognize the well interference. Lawal et al[17] demonstrated rate transient analysis tools can be used to model fracture hits, and examples from Haynesville and Marcellus were examined.

Thompson[18] presented a semianalytical superposition model for analyzing pressure, and rate data from wells where production characteristics were altered because of the interference from nearby fracture operations. Yu et al[19] established a physical model to simulate the well interference of shale gas wells by embeded discrete fracture model (EDFM) and analyzed the effects of fracture connectivity and matrix permeability. Tang et al[20] developed a comprehensive compositional reservoir model to study the well interference phenomena in the Eagle Ford Shale/Austin Chalk production system. Wang et al[21] studied the transient pressure simulation of well interference communicated by connecting fracture (ie, fracture hit) during interference testing of wells with variable operating conditions. Gao et al[22] used numerical simulation methods to study the sensitivity of well test parameters in gas reservoir horizontal wells and explained the formation parameters upon pressure recovery test.

The three methods possess their own advantages, among which pressure transient analysis (PTA) method applies downhole pressure monitoring data collected in the field, which can more accurately identify the interwell interference and judge the interference intensity. It is urgent to profoundly study the transient pressure behaviors of shale gas MFHWs with neighboring wells, considering the complex fracture network and the multi-flow mechanism, such as the desorption and diffusion of shale gas,[23,24]

To study the porous media flow and transient pressure behaviors of shale gas MFHWs, many scholars have established kinds of multi-linear flow region coupled models, including three-region, five-region and seven-region coupled model. Before this, Bello and Wattenbarger[25] used the layered double porosity model and the Warren-Root dual-porosity model to analyze the pressure response and production dynamics of MFHWs in shale reservoirs. However, those two dual-porosity reservoir models are too simplified to characterize the fracture network after multi-stage fracturing. Therefore, Ozkan et al[26] and Al-Rbeawi[27] divided the stimulated shale reservoirs into HFs, SRV, and matrix. Moreover, they simplify the flow in these three regions into the one-dimensional linear flow by establishing a three-linear-flow model. Additionally, Stalgorova and Mattar[28] and Zhang et al[29] improved the three-linear-flow model by considering the unstimulated areas between two hydraulic fracturing SRV and proposed a five-region coupled flow model. Zeng et al[30] further subdivided the five-region coupled flow model and proposed a seven-region coupled flow model. Based on these coupled models, Wang et al[31] and Kim et al[32] analyzed the stress-sensitive effects of gas reservoirs and fractures. Xiao et al[33] presented a new semi-analytical methodology for pressure transient analysis of multi-well-pad-production scheme in shale gas reservoirs. Overall, the flow around shale MFHWs is mainly characterized by coupled linear flow models with multiple subdivided regions. In these models, HF, SRV, and matrix are commonly applied, and they are separately discussed as follows. The flow in fracturing fractures usually satisfied Darcy law or high-speed non-Darcy law.[34] The SRV can be treated as dual media or characterized by complex fracture network models.[35] The matrix can be regarded as a homogenous ultra-low-permeability medium. However, some scholars treat it as a dual medium with natural fracture network.[36] The equivalent permeability can be analyzed in the multiple regions coupled model to simplify the effects of desorption and diffusion in the SRV and matrix. From these three main regions, five regions or seven regions are further subdivided, but the physical parameters in the added regions are difficult to obtain.

Well interference has had a significant influence on the SRV interpretation. It has drawn scholars' attention in recent years, but its impact on transient behaviors is rarely reported. Researchers generally ignore the well interference in the longitudinal direction, and the existing well interference research method cannot accurately determine the specific interference fracturing segment and the numerical simulation analysis of the interference well group. The problems shown in previous literature mainly include the following three aspects.

1. There is no detailed discussion on the pressure interference between the fracture sections of the active well and observation well;
2. There is no quantitative evaluation on the interference intensity between the fractured sections and between wells;
3. Analytical models and methods for shale gas interference well test data need to be improved.

Considering these problems above, we present a comprehensive analysis of the well interference of the practical MFHW group of the Jiaoshiba shale gas field in this paper. This research may help to determine the well interference between lower and upper shale gas layers and provide some foundations to optimize upper layers' gas production performance.

The rest contents of this paper are arranged as follows: in Section 2, an analysis process of MFHW interference is put forward, and it is divided into three phases, which are discussed in the following three sections based on Jiaoshiba shale gas field. In Section 3, the observation wells' BHP responses are analyzed during a neighboring well fracturing, and the interference stages and strength are determined. Section 4 provides the scheme and data of well interference, and a numerical analysis method is presented. Section 5 analyzes the dynamic production of an MFHW group. The paper is concluded in Section 6.

2 | MFHW INTERFERENCE ANALYSIS PROCESS

The shale gas well interference analysis process includes observation well's bottom-hole pressure response analysis (BHPRA) during the fracturing of neighboring well, BHPRA of well interference test, and production dynamic analysis, as shown in Figure 1. Overall, the analysis process contains three phases as follow.

1. Analyzing the observation MHFW's BHP response during the fracturing of neighboring infilling well. Bottom-hole pressure response analysis can determine the fracturing stages of observation wells that connected with neighboring wells and distinguish the disconnected stages. Especially, interference strength can be calculated according to pressure response amplitude.
2. Bottom-hole pressure response analysis of well interference test. It aims at understanding observation MFHWs' pressure disturbance caused by their neighboring active MFHWs' production variation. When adjusting the active MFHW's production system (open/close well), the pressure response time delay of the observation MFHWs reflects the pressure diffusion in the dominant communicated region. The pressure response amplitude caused by their neighboring MFHWs' production variation reflects the interference strength.
3. Production dynamic analysis. When adjusting the production system, the well interference of A MFHW group is monitored directly by testing dynamic wellhead pressure and gas/water production. Production dynamic analysis can further verify the existence of well interference.

3 | BHPRA DURING THE FRACTURING OF NEIGHBORING WELL

A well group is a shale gas MFHW group locates at the Ordovician Wufeng and Silurian Longmaxi Formation of Jiaoshiba shale gas field, including three wells A-1, A-2 (parent wells), and A-3 (child infilling well). A-1 and A-2 well drill through the lower 1-4 layers with 13 and 17 stages of hydraulic fracturing, and A-3 well drills through the upper 7-9 layers with 18 stages of hydraulic fracturing, as shown in Figure 2.

The Longmaxi Formation of the Silurian is a deep-water continental shelf deposit with a sizeable gas-bearing shale (thickness 93 m), organic matter abundance 2.54%, vitrinite

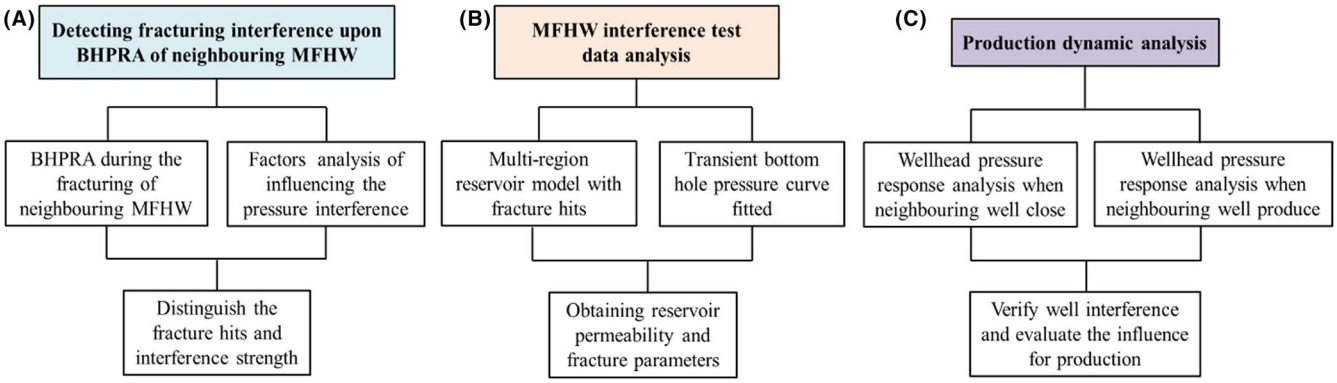

FIGURE 1 Shale gas multi-stage fracturing horizontal wells (MFHWs) interference analysis process

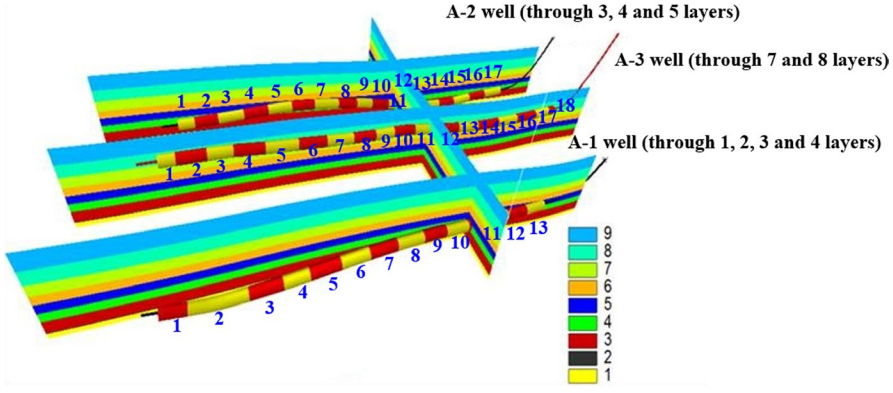

FIGURE 2 Fracturing stages and layers of A well group (A-1 well perforated 13 stages and operated hydraulic fracturing, A-2 well perforated 17 stages and operated hydraulic fracturing, and A-3 well perforated 18 stages and operated hydraulic fracturing)

reflectance 2.5%, brittle mineral content 56.53%, and gas content 2-6 m^3/ton. The lower quality shale gas layers are 40 m thick, the organic matter abundance is 3.03%, the porosity is 4.8%, and the gas content is 5-6 m^3/t. We use the steady-state method to test the shale reservoir permeability. The horizontal permeability (contains matrix and natural fractures) is mainly 0.001-355 mD with obvious heterogeneity. The matrix permeability is generally lower than 1 mD, almost 0.0015-5.71 mD. The longitudinal stratification has a significant contribution to the horizontal seepage capacity of the formation.

Prehydrochloric acid treatment is used before fracturing to reduce fracturing pressure. The ceramsite is chosen as the proppant to improve the fracture conductivity and connectivity, and to increase the effective stimulating reservoir volume (SRV).

The hydraulic fracturing of neighboring wells provides quite strong interference signals. The high-precision electronic pressure gauge, installed in the later stage of the well shut-off, can receive the interference signals of neighboring well fracturing. These signals are shown in the pressure transient monitored. The BHP of parent wells (A-1 and A-2) and pump rate (PA) of child well (A-3) are shown in Figure 3. According to the pressure response of the well during the fracturing of each neighboring well, the connected fractures between the two wells is determined. The comprehensive fracturing data and the horizontal well trajectory data are used to explore the cause of interference response during the fracturing of neighboring well. According to the amplitude of the different pressure response signals, the interference strength between two wells' hydraulic fracturing stages can be qualitatively determined. This provides a basis for the establishment of geological models to understand well interference and analyzes them step by step to obtain detailed results.

During the fracturing of the child well, the BHP responses of the parent wells are shown in Figure 3. From the BHP of A-2 well (red line), the interference responses are significant after the third and fourth fracturing stages of A-3 well, and there is almost no pressure response of A-1 well as shown in its BHP curve (blue line). The pressure interference responses of wells A-1 and A-2 are common obvious when A-3 well operated the hydraulic fracturing at the seventh and eighth stages. The main reason for the apparent pressure interference response is the nearer well distance between the front fracturing stages of A-2 and A-3 (260 m). However, increasing fracturing scale (injection sand volume and liquid volume, as shown in Table 1) is the key for the existing of apparent pressure interference response during the seventh, eighth, and ninth stages of A-3 well. According to this, it can be preliminarily judged that there may be fractures hits in the third, fourth, seventh, and eighth stages. The pressure interference caused by the fracture hits needs to be further evaluated in the gas production system adjustment.

4 | WELL INTERFERENCE TEST

4.1 | Test scheme

Interference test was carried out on A well group in Feb 2017. Three wells installed downhole pressure gauges for BHP monitoring. The whole test contains three parts: (a) well clean-up with a high gas rate; (b) well shut-in pressure recovery; and (c) interference test. During the interference test, A-3 well operated twice open-well production with 12×10^4 m^3/d gas rate, and parent wells keep shut-in, the test scheme is shown in Table 2.

4.2 | Test results

The interference test pressure is shown in Figure 4. From the pressure curve fluctuation characteristics, the pressure recovery ability of well A-1 is strong, and its pressure drop caused by A-3 well production is weaker. In contrast, the pressure recovery ability of well A-2 is weak, and its pressure drop

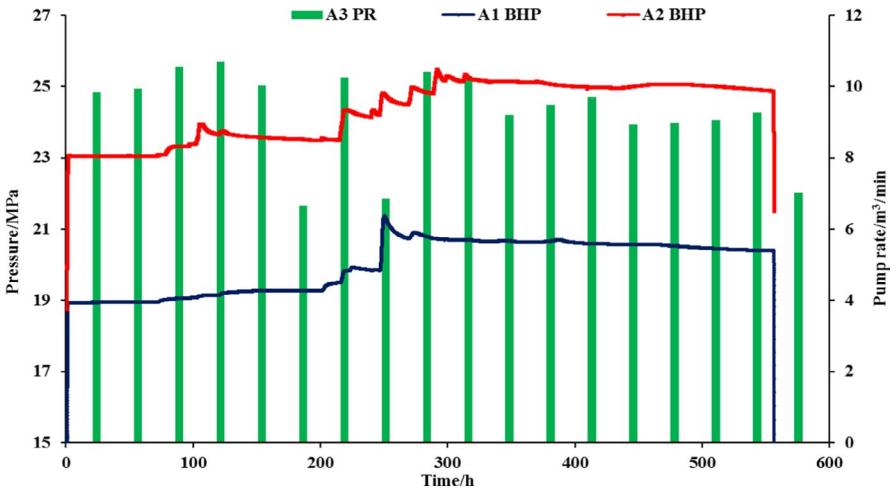

FIGURE 3 Interference pressure response of neighboring wells in A well group

TABLE 1 BHP response of A-1/A-2 well during A-3 hydraulic fracturing

	A-3 well fracturing parameters								Fracturing parameters					
A-3 FS	FP/MPa	PP/MPa	PSP/MPa	PR/m^3	IL/m^3	IS/m^3	NFS of A-1/A-2	PRA/MPa	FP/MPa	PP/MPa	PSP/MPa	PR/m^3	IL/m^3	IS/m^3
1st	70.82	53.68-68.84	29	12.0-14.0	1871.4	75.21	A-1 1st	0.003	79.3	77.0-87.0	44.5	11	2224.6	0.14
2nd	65.21	52.32-70.52	31	14	1856.6	74.35	A-1 2nd	0.008	87.2	79.8-87.0	38	1.0-12.5	1664.9	0.35
							A-2 1st	0.006	86.7	63.2-86.3	47.6	4.0-8.0	1348	0.29
3rd	65.94	53.21-65.57	31	14	1775.9	77.18	A-1 2nd	0.036	87.2	79.8-87.0	38	1.0-12.5	1664.9	0.35
							A-2 3rd	0.034	87.8	68.1-83.4	43.1	0.9-9.0	1430	0.35
4th	71.2	57.13-72.79	33	14	1856.2	71.32	A-1 3rd	0.031	79.7	77.0-87.5	57	10	1732.3	1.82
							A-1 4th		84.7	80.0-87.0	42	7.0-10.0	1530.9	0.25
							A-2 3rd	0.224	87.8	68.1-83.4	43.1	0.9-9.0	1430	0.35
							A-2 4th		88	74.0-90.0	41.2	1.0-10.0	1247	0.7
5th	78.46	54.08-78.46	31	14	1880.7	78.27	A-1 5th	0.018	88.6	60.0-85.5	36.7	2.0-8.0	1631.89	/
							A-2 5th	0.068	86.5	55.0-83.0	49	6.5-9.0	1860.9	10.7
6th	73.78	54.22-75.44	36	14	1931.4	74.73	A-1 5th	0.046	88.6	60.0-85.5	36.7	2.0-8.0	1631.89	/
							A-2 6th	0.566	74.1	72.7-82.8	39.1	0.9-8.0	1737.82	42.92
							A-2 7th		86.9	44.9-86.1	32.5	0.9-8.0	2069	40.1
7th	69.37	51.11-68.47	32	14	1976.1	75.17	A-1 6th	0.065	92.5	32.3-92.5	31.7	2.0-10.0	2203.6	43.06
							A-1 7th		75.4	77.0-87.0	33.9	11	1647	45
							A-2 7th	0.088	86.9	44.9-86.1	32.5	0.9-8.0	2069	40.1
8th	78.85	62.3-74.7	31	14	1834.1	75.09	A-1 8th	0.141	78.5	41.4-78.1	37.7	10.0-14.0	2302.7	36.74
							A-2 8th	0.06	89.79	49.64-89.79	31.6	10.0-14.0	2174	65.06
9th	75.82	54.21-71.62	36.54	14	1810.4	75.27	A-1 8th	0.351	78.5	41.4-78.1	37.7	10.0-14.0	2302.7	36.74
							A-2 9th	0.859	93	50.8-68.4	33.8	10.0-14.0	1860.4	40.47
10th	73.62	55.58-75.22	31.6	13	1737.1	74.05	A-1 9th	0.09	85	45.3-95.0	35	2.0-14.0	1419.8	0.47
							A-2 10th	0.002	90.8	60.8-75.5	36.4	8.0-13.5	1536.52	14.8
11th	60.07	52.42-85.78	32	10.5-12.0	1504.8	42.25	A-1 9th	0.014	85	45.3-95.0	35	2.0-14.0	1419.8	0.47
							A-2 11th	0.189	77.3	44.5-93.6	32.8	7.0-8.0	1797.5	42.68
							A-2 12th		88.9	43.7-68.4	28.5	10.0-12.0	1931.2	60
12th	55.12	44.97-71.34	26	12	1470.2	62.4	A-1 11th	1.505	72	44.0-62.0	27	14	1958.2	70.5
							A-2 13th	0.599	82.91	51.29-81.39	33.1	13.0-13.0	1977.92	60.6

(Continues)

TABLE 1 (Continued)

A-3 well fracturing parameters								Fracturing parameters					
A-3 FS	FP/MPa	PP/MPa	PSP/MPa	PR/m^3	IL/m^3	IS/m^3	NFS of A-1/A-2	PRA/MPa	FP/MPa	PP/MPa	PSP/MPa	PR/m^3	IL/m^3	IS/m^3
13th	56.93	45.42-57.08	27	12	1684	75.96	A-1 12th	0.169	65.4	44.3-65.5	28.8	2.0-14.0	1858	71.23
							A-2 14th	0.477	89.2	44.3-77.0	27.7	4.5-12.0	1874.1	61.1
14th	62.04	48.73-86.96	26	12	1565.9	76.5	A-1 13th	0.169	65.8	35.1-64.2	29.4	14	1910	71.17
							A-2 15th	0.648	80.18	50.53-72.28	27.63	8.5-13.0	1815.47	55.21
15th	56.48	45.92-75.05	28.47	12	1363.8	66.23	A-2 16th	0.126	81.5	44.7-65.7	29.2	8.5-14.0	1673	62.08
16th	56.43	45.55-57.1	26	12	1365.1	69.24	A-2 16th	0.201	77.73	55.12-91.17	62.98	3.5-9.5	1315.53	11.37
17th	55.02	55.52-67.82	34	12	1487.8	64.42	No NFS of A-1/A-2							
18th	74.45	54.67-87.03	42	10.0-12.0	1052.7	26.79	No NFS of A-1/A-2							

Abbreviations: BHP, bottom-hole pressure; FP, fracturing pressure; FS, fracturing stages; IL, injection liquid; IS, injection sand, NFS, neighboring fracturing stages; PP, pump pressure; PR, pump rate; PRA, pressure response amplitude; PSP, pump-stop pressure.

caused by A-3 well production is stronger. In order to quantify the well interference, the pressure response time delay caused by the well opening/closing during the interference test is counted, according to PRA. Pressure response amplitudes of different interference stages are calculated as shown in Table. 3.

4.3 | Numerical simulation analysis

4.3.1 | Model description

According to the geological data and logging interpretation results, the fundamental mechanism geological model is established. Based on the multi-region coupling flow model, the numerical well test method is used to fit the pressure recovery test data of three wells to explain the reservoir, wellbore, and fracture parameters. By the well-fitted curve fitting model, the actual fitting of the production dynamic data is further carried out. By repeatedly fitting the well testing curve and the dynamic production data, a more reliable numerical model is finally obtained. The well interference can be observed not only according to the impact on the pressure field, but also can predict the production capacity of the horizontal wells group. According to the numerical simulation model established by Gao et al,[22] the modeling area is mainly divided into three parts.

Due to the significant difference in porosity and permeability between the fracturing and unfracturing areas in the reservoir, shale reservoirs around MFHWs are divided into subregions, including HFs, SRV with abundant inducing microfractures, and matrix as shown in Figure 5. Assumptions: (a) Water flow is ignored, and there is only single-phase gas flow existed in each subregion. (b) Just viscous flow exists in the HF and satisfies the Darcy law,[37] neglecting the longitudinal flow. (c) SRV is treated as dual media, and each hydraulic stage's SRV overlaps with each other in one MFHW. (d) Matrix is regarded as homogeneous ultra-low permeability media. (e) Pseudopressure function ($\boldsymbol{m}$) is introduced to simplify the gas composition change with temperature and pressure.[38] (f) There are three connection modes between the well and neighboring wells, including the connection of inducing microfracture clusters in the SRV and the connection of HFs as shown in Figure 5.

4.3.2 | Mathematical model

Pseudopressure

For the actual situation of the gas reservoir, especially during the regular mining of the gas field, the gas viscosity and the compression factor are functions of the pressure. To make the gas flow equation reflect the actual situation of the shale

TABLE 2 Interference test scheme of A well group

Well	Well clean-up with high gas rate	Well shut-in pressure recovery	Interference test		
			1st stage	2rd stage	3rd stage
A-3	14 d, 12×10^4 m^3/d	20 d	Gas producing 3 d, 12×10^4 m^3/d	Well shut-in 3 d	Gas producing 3 d, 12×10^4 m^3/d
A-1	14 d, 8×10^4 m^3/d	20 d	Well shut-in		
A-2	14 d, 8×10^4 m^3/d	20 d	Well shut-in		

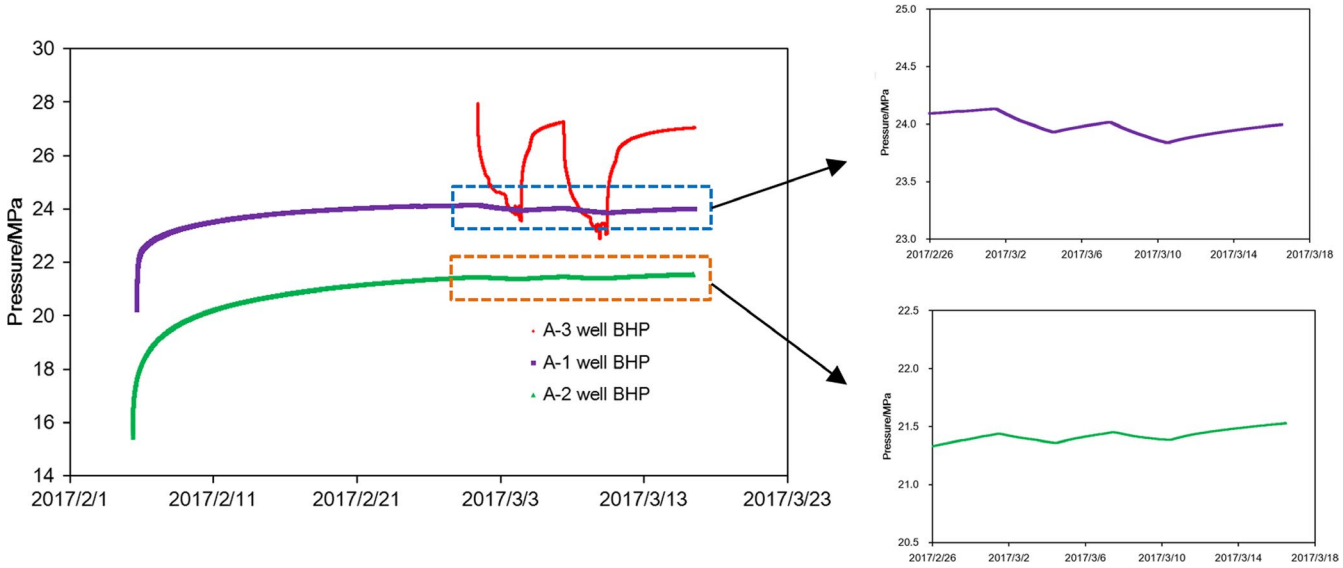

FIGURE 4 Interference test pressure curve. BHP, bottom-hole pressure

gas reservoir, we use the real gas pseudopressure, ***m(p)*** of Al-Hussainy et al,[39] which takes into account the variations of gas viscosity and Z-factor as a function of pressure.

$$m(P) = 2\int_{p_0}^{p} \frac{p}{\mu(p)\cdot z(p)}\mathrm{d}p, \tag{1}$$

where p is reservoir pressure, MPa; p_0 is initial reservoir pressure, MPa; μ is gas viscosity, mPa s; z is compressibility coefficient, dimensionless.

HF flow model

It is assumed that fluid exchanges exist among the fracture, the SRV and the wellbore, the boundary between the well and HFs is defined as Γ_1, and the boundary between the SRV and the HFs is Γ_2. If the HFs directly connected in one well pair, the fluid exchange between two wells' HFs needs to be considered. Commonly, Shale gas wells produce at a given production rate first according to the development scheme, and the gas supply capacity of the reservoir gradually tends to insufficient as the pressure continues to drop. The shale gas wells are converted to produce with constant pressure later. Based on this, the flow equations in the finite conductivity fractures are established by Gao et al[22] as follows.

$$\nabla^2 m_\mathrm{F} = \frac{\phi_\mathrm{F} c}{k_\mathrm{F}}\frac{\partial m_\mathrm{F}}{\partial t}. \tag{2}$$

The initial conditions:

$$m_\mathrm{F}\big|_{t=0} = m_i. \tag{2a}$$

The inner boundary condition: 1. Constant pressure boundary conditions:

$$m_\mathrm{F}\big|_{\Gamma_1} = m_\mathrm{w}. \tag{2b}$$

1. Fixed output boundary conditions:

$$\sum -\frac{k_\mathrm{F}}{\mu}\frac{\partial m_\mathrm{F}}{\partial n}\bigg|_{\Gamma_1} = C_\mathrm{w}\frac{\partial m_\mathrm{F}}{\partial t} + \frac{2p_\mathrm{sc}T}{\mu Z_\mathrm{sc}T_\mathrm{sc}}q_\mathrm{iw,F}. \tag{2c}$$

The outer boundary condition:

$$m_\mathrm{S,f}\big|_{\Gamma_2} = m_\mathrm{F}\big|_{\Gamma_2}. \tag{2d}$$

TABLE 3 Interference test analysis of A well group

MFHW	Stimulating signal		Date	Time	Pressure/MPa	Pressure response time delay/h	Pressure response amplitude/MPa
A-1	(1)	Well opening	2017/3/1	11:58:32	21.439	1.65	0.0808
	(2)	Well shut-in	2017/3/4	12:28:32	21.3582	1.17	0.0938
	(3)	Well opening	2017/3/7	12:07:47	21.452	1.83	0.0681
	(4)	Well shut-in	2017/3/10	12:16:17	21.3839	1.16	0.1426
A-2	(1)	Well opening	2017/3/1	11:24:55	24.1331	1.09	0.2048
	(2)	Well shut-in	2017/3/4	12:31:55	23.9283	1.22	0.0868
	(3)	Well opening	2017/3/7	11:43:40	24.0151	1.43	0.1791
	(4)	Well shut-in	2017/3/10	12:14:55	23.836	1.14	0.1559

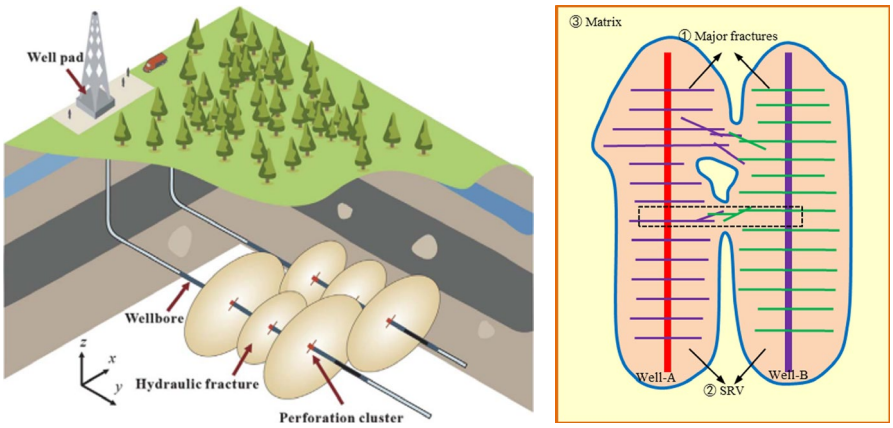

(A) MFHW fracture hit 3D schematic. **(B)** MFHW fracture hit 2D schematic.

FIGURE 5 Multi-region coupled shale reservoir physical model (Well A and well B are two multi-stage fracturing horizontal wells (MFHWs), the hydraulic fractures connected with the stimulated reservoir volumes (SRVs), and the SRVs are dual medium. A, MFHW fracture hit 3D schematic. B, MFHW fracture hit 2D schematic

where m_F is the gas pseudopressure of HF, MPa^2/(mPa s); t is time, day; φ is porosity, dimensionless; k is permeability, mD; n is normal direction mark, dimensionless; F is HF mark, dimensionless; sc is standard condition mark, dimensionless; c is gas compressibility factor, MPa^{-1}; C_w is wellbore storage factor, m^3/MPa; $q_{iw,F}$ is the fluid exchange volume between the HF and wellbore, m^3/d.

SRV flow model

Matrix system flow model. Assuming that gas desorbed from the SRV matrix system, the desorption gas satisfies the Langmuir isothermal adsorption equation on the surface of the matrix bedrock. The migration of gas includes viscous flow, Knudsen diffusion, and surface diffusion. Hence, the matrix system flow model is Equation (3).

$$\nabla^2 m_{S,m} - \alpha(m_{S,m} - m_{S,f}) = \left[\frac{\phi_{S,m} c}{k_{S,m}} + \frac{2R_g T \rho_s V_{S,L}(1-\phi_{S,m})}{k_{s,m} V_{st}(m_{S,L}+m_{S,m})^2}\right] \frac{\partial m_{S,m}}{\partial t}. \quad (3)$$

where $m_{S,m}$ and $m_{S,f}$ are the gas pseudopressure of the SRV matrix system and fracture system, respectively, MPa^2/(mPa s); S is SRV mark, dimensionless; m and f are the marks of SRV matrix system and fracture system, respectively, dimensionless; $V_{S,L}$ is Langmuir gas volume, m^3/kg; V_{st} is gas molar volume at standard temperature and pressure conditions, m^3/kmol; $m_{S,L}$ is Langmuir gas pressure, MPa^2/(mPa s); T is reservoir temperature, K; R_g is gas constant, J/mol/K.

Fracture system flow model. Because the microfractures in the SRV region are very developed, how to characterize the fracture network equivalently in the seepage model has been a difficult problem to solve. For this reason, many scholars hypothesize that the development and spread of fracture networks satisfy the fractal characteristics and propose a fractal model that characterizes natural fracture networks.[40-42] However, the critical parameters such as the fractal dimension in the model are difficult to determine. Also, considering complex networks will greatly increase the complexity of meshing and numerical calculations. Therefore, the equivalent permeability is used to characterize the comprehensive permeability of the fracture system in the SRV region. The gas in the fracture medium in the SRV is mainly in the form of free gas. Therefore, only the viscous gas flow and Knudsen diffusion are considered in the fracture medium, and the apparent permeability $\boldsymbol{k}_{s,f}$ is used to represent the permeability of the fracture medium.[43]

$$k_{S,f}=\frac{b^3}{12c}(1+\beta K_n)\left(1+\frac{4K_n}{1+K_n}\right), \quad (4)$$

where K_n is Knudsen number, dimensionless; β is tenuity factor, dimensionless; b is average fracture aperture, m; and c is average fracture spacing, m.

Assume that the wellbore only has fluid exchange with the fracture, neglecting the direct fluid exchange between the fracture system and the wellbore in the SRV, and defining the interface between the fracture and the matrix systems in the SRV as Γ_3. Then, the flow model in the fracture system of the SRV is presented as Equation (5).

$$\nabla^2 m_{S,f}+\alpha(m_{S,m}-m_{S,f})=\frac{\phi_{S,f}c}{k_{S,f}}\frac{\partial m_{S,f}}{\partial t}. \quad (5)$$

The initial conditions：

$$m_{S,m}\big|_{t=0}=m_{S,f}\big|_{t=0}=m_i. \quad (5a)$$

Inner boundary condition：

$$m_{S,f}\big|_{\Gamma_2}=m_F\big|_{\Gamma_2}. \quad (5b)$$

Outer boundary condition：

$$m_{S,f}\big|_{\Gamma_3}=m_M\big|_{\Gamma_3}. \quad (5c)$$

where α is exchange flow coefficient, (m^3 mPa s)/MPa^2; M is matrix mark, dimensionless.

Matrix flow model

The shale gas reservoir is rich in kerogen organic matter, and the hydrocarbon gas generated in the kerogen satisfies the saturation adsorption and then spreads from the kerogen pores to the inorganic matrix pore space where the hydrocarbon concentration is relatively reduced. The gas in the kerogen occurs in two forms: free gas and adsorbed gas. The pores in the kerogen have the same order of magnitude as the gas molecules in the shale gas. Therefore, the free gas will generate Knudsen Diffusion in the kerogen nanoporous network. At the same time, the kerogen is saturated with a large amount of adsorbed gas, and the adsorbed gas on the surface of the skeleton will produce surface diffusion. Assuming that the shale gas reservoir is isothermally developed, the Langmuir isotherm adsorption equation is used to describe the adsorption and desorption of kerogen.

The apparent permeability of the matrix region proposed by Singh et al[44] and Civan et al[45] is:

$$k_{M,a}=k_0\left[1+\frac{128}{15\pi^2}\tan^{-1}\left(4K_n^{0.4}\right)K_n\right]\left[1+\frac{4K_n}{1+K_n}\right]. \quad (6)$$

Thus, the kerogen-medium continuity equation considering Knudsen diffusion, adsorption-desorption, and surface diffusion is obtained as Equation (7).

$$\nabla^2 m_M=\frac{\phi_M c}{k_{M,a}}\frac{\partial m_M}{\partial t}. \quad (7)$$

The initial conditions：

$$m_M\big|_{t=0}=m_i. \quad (7a)$$

Inner boundary condition：

$$m_{S,f}\big|_{\Gamma_3}=m_M\big|_{\Gamma_3}. \quad (7b)$$

Outer boundary condition：

$$\left.\frac{\partial m_M}{\partial n}\right|_{\Gamma_4}=0. \quad (7c)$$

4.3.3 | Interference numerical analysis

The finite volume method of MATLAB software was used to solve the mathematical model. The input parameters in the model are reservoir thickness 89m, gas relative density 0.5642, porosity 4.98%, reservoir temperature 188.6 K, well radius 69.85 mm, A-1 well horizontal length 1200 m, A-2 well horizontal length 1434 m, and A-3 well horizontal length 1520 m. In the initial calculation, the reservoir permeability is assumed to be 0.1 mD, and the fractures' half-length in each well is given the same average length of 65 m. The interference test data are fitted by continuously adjusting the permeability of the model and the conductivity of the fractures. The curve fitting results are shown in Figure 6.

Through fitting the pressure test data in Figure 6, reservoir permeability, fractures conductivity, and half-length are interpreted. The reservoir permeability is 0.043 mD, average fractures conductivity of A-3 well is 1524 mD m, average fractures conductivity of A-2 well is 673 mD m, and average fractures conductivity of A-1 well is 750 mD m. The fractures' half-length of three wells are shown in Table. 4.

The fracture half-length is set before the calculation, and the half-length determines the boundary of the high-permeability region of the HF (Equations 1 and 2, Γ_1). By comparing the calculated pressure with the test pressure, the fracture half-length is determined after multiple fittings.

5 | PRODUCTION DYNAMIC ANALYSIS

Wellhead pressures are continuously recorded during all completions and flowback operations. The rate of pressure

buildup plus the magnitude and frequency of the interwell hits are studied. Pressure hits are then compared with production interactions between wells. Connections are mapped to form a comprehensive image of the fracture network. In the pad studied, all wells had multiple hits with varying degrees of communication across the fracture network. Observations confirm that fractures had significant vertical and lateral growth establishing a highly complex network. Interference analysis indicates the connections between wells often diminish over time. As a final validation, the high degree of interaction and fracture overlap are shown to be consistent with high-resolution microseismic observations. Establishing the extent of the effective fracture network is fundamental to deciding design variables. Multi-variable pad designs and production results can only be deciphered when viewed in conjunction with fracture interactions. The process discussed provides a simple way to observe and understand these interactions.

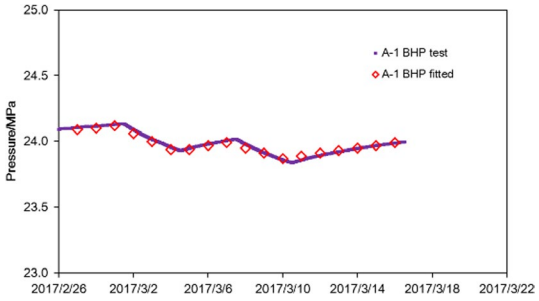

(A) A-1 pressure test data and fitted data.

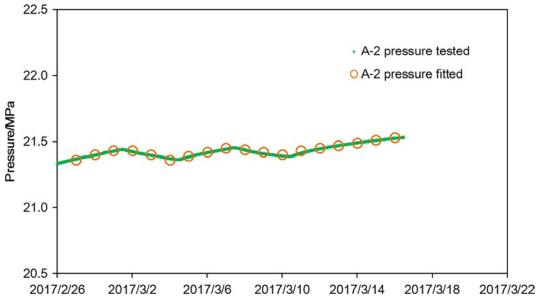

(B) A-2 pressure test data and fitted data.

FIGURE 6 Numerical simulation results of pressure test and data fitted. a. A-1 pressure test data and fitted data. b. A-2 pressure test data and fitted data

The cumulative gas productions of parent A-1 and A-2 well are 3318.13 × 10^4 m^3 and 2941.53 × 10^4 m^3, respectively, and the average daily gas production is 64 900 and 60 500 m^3/d. Their casing pressure reduced from 32 to 33.0 MPa at the initial stage of production to 12.9-14.6 MPa at July 2017. A-3 put into production at February 2016, and its average daily gas production of A-3 well is 65 300 m^3/d. All of these three wells have experienced many times open/close well.

In March 2017, the gas production of wells A-1 and A-3 was stable at around 6 × 10^4 m^3. After the interference test, all three wells produced at around 6 × 10^4 m^3 for 20 days. After that, A-2 well shut down, but A-1 and A-3 wells still produced at a daily gas production rate of 6 × 10^4 m^3, which led to a pressure drop during the later pressure recovery of A-2 well, as shown in Figure 7.

TABLE 4 Fractures' half-length of three wells

A-3 well HF stages	Half-length/m	A-1 well HF stages	Half-length/m	A-2 well HF stages	Half-length/m
1st	85	1st	16	1st	12
2nd	84	2nd	8	2nd	14
3rd	87	3rd	20	3rd	18
4th	80	4th	15	4th	22
5th	88	5th	22	5th	33
6th	84	6th	48	6th	48
7th	84	7th	51	7th	45
8th	84	8th	41	8th	73
9th	85	9th	21	9th	45
10th	83	10th	23	10th	17
11th	47	11th	79	11th	48
12th	70	12th	80	12th	67
13th	85	13th	80	13th	68
14th	86			14th	69
15th	74			15th	62
16th	78			16th	70
17th	72			17th	67
18th	30				

Abbreviation: HF, hydraulic fracture.

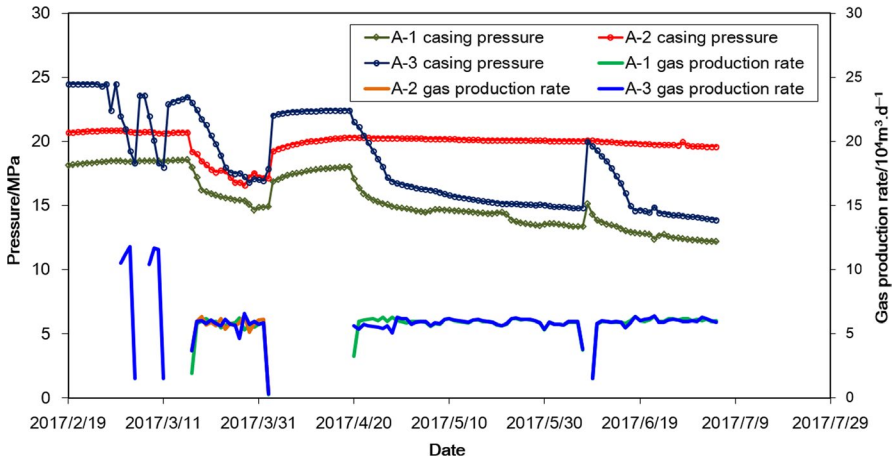

FIGURE 7 A well group production data (the whole production history contains two parts, part I is the interference test, and part II is the normal production period)

The bottom-hole pressure is calculated by the model in this paper, and the monitoring of the bottom-hole pressure requires the installation of a high-precision pressure gauge. The pressure of production data is casing pressure recorded in wellhead. Because the pressure loss in the wellbore cannot be accurately calculated, it is impossible to accurately simulate the casing pressure data of the wellhead. In the follow-up study, the investigation on wellbore pressure loss will be further carried out to better adjust the fitting model parameters and to improve the model.

6 | CONCLUSIONS

In recent years, with the continuous expansion of the shale gas wells pattern's scale and reduction in well spacing, the problem of well interference has become increasingly serious. The new drilled MFHW in upper gas layers has an impact on the output of the MFHW in lower gas layers of Jiaoshiba, but it is beneficial to increase the gas production of the gas field through the development of multi-well layers. The longitudinal interference between the upper gas layers and the lower gas layers of Jiaoshiba was evaluated by the proposed comprehensive evaluation method. The interference fracturing stages between the two wells were found by the fracturing interference detecting, and the interference strength was quantitatively evaluated by the pressure response amplitude. Whether water production increases sharply determines whether fracture hits exist, which is helpful for understanding the longitudinal extension of the HFs and the pollution of the shallow groundwater.

Through well interference test, we found that the parent wells are disturbed by the child wells when adjusted production system. The pressure interference is evaluated by the daily pressure drop during the multi-well production in the upper and lower layers. The well interference exists in the multi-well production system.

To study the transient pressure behaviors of shale gas MFHW under well interference, we establish a multi-region coupled flow model based on the pore fracture structures and flow mechanisms of the different region. Then, perpendicular bisection (PEBI) grids and finite volume method are used for the numerical solution. Utilizing the measured shut-in pressure recovery test data of shale gas wells, we explain the property parameters of the reservoir and HFs. Moreover, BHP data monitored in the later stage are fitted to verify the accuracy of the model. Based on the shale gas seepage model, the pressure field and BHP are analyzed under the disturbance of neighboring wells.

ACKNOWLEDGMENTS

The study was supported by Open Fund (PLN201711) of State Key Laboratory of Oil and Gas Reservoir Geology and Exploitation (Southwest Petroleum University), National Natural Science Foundation of China (11702300) and PetroChina Innovation Foundation (2017D-5007-0208).

ORCID

Dapeng Gao https://orcid.org/0000-0001-8813-7041

REFERENCES

1. Ma XH, Xie J. The progress and prospects of shale gas exploration and development in southern Sichuan Basin, SW China. *Petrol Explor Dev*. 2018;45(1):161-169.
2. Zou CN, Yang Z, He DB, et al. Theory, technology and prospects of conventional and unconventional natural gas. *Petrol Explor Dev*. 2018;45(4):1-13.
3. Yi JZ, Bao HY, Zheng AW, et al. Main factors controlling marine shale gas enrichment and high-yield wells in South China: a case study of the Fuling shale gas field. *Mar Petrol Geol*. 2019;103:114-125.
4. Ilkay U, Basak K, Hossein K. Multiphase rate-transient analysis in unconventional reservoirs: theory and application. *SPE Reserv Eval Eng*. 2016;19(4):1-14.
5. Soeder DJ. The successful development of gas and oil resources from shales in North America. *J Petrol Sci Eng*. 2018;163:399-420.

6. Ajani AA, Kelkar MG. Interference study in shale plays. Paper SPE 151045 presented at: SPE Hydraulic Fracturing Technology Conference; 2012; The Woodlands, TX, USA.
7. Manchanda R, Sharma MM, Holzhauser S. Time-dependent fracture-Interference effects in pad wells. *SPE Prod Oper*. 2014;29(4):1-14.
8. Sardinha C, Petr C, Lehmann J, Pyecroft J, Merkle S. Determining interwell connectivity and reservoir complexity through Frac pressure hits and production interference analysis. Paper SPE 171628 presented at: the SPE/CSUR Unconventional Resources Conference; 30 September to 2 October, 2014; Calgary, AB, Canada.
9. Vidic RD, Brantley SL, Vandenbossche JM, Yoxtheimer D, Abad JD. Impact of shale gas development on regional water quality. *Science*. 2013;340(6134):1235009.
10. Najurieta HL. A new interference test method for high-precision diffusivity distribution measurements. Paper SPE 28379 presented at: SPE Annual Technical Conference and Exhibition; September 25–28, 1994; New Orleans, LA.
11. Mezghani M, Roggero F. Combining gradual deformation and upscaling techniques for direct conditioning of fine scale reservoir models to interference test data. *SPE J*. 2004;9(1):79-87.
12. Marongiu-Porcu M, Lee D, Shan D, Morales A. Advanced modeling of interwell—fracturing interference: an eagle ford shale-oil study. *SPE J*. 2015;21(5):1567-1582.
13. Yaich E, Souza OCDD, Foster RA, Abou-Sayed IS. A methodology to quantify the impact of well interference and optimize well spacing in the Marcellus shale. Paper SPE 171578 presented at: the SPE/CSUR Unconventional Resources Conference; 30 September to 2 October, 2014; Calgary, AB, Canada.
14. Pang W, Ehlig-Economides CA, Du J, He Y, Zhang T. Effect of well interference on shale gas well SRV interpretation. Paper SPE 176910 presented at: SPE Asia Pacific Unconventional Resources Conference and Exhibition; November 9-11, 2015; Brisbane, Qld, Australia.
15. Liang BS, Khan S, Tang YL. Fracture hit monitoring and its mitigation through integrated 3D modeling in the Wolfcamp stacked pay in the midland basin. Paper URTeC 2671336 presented at: the Unconventional Resources Technology Conference; July 24-26, 2017; Austin, TX, USA.
16. Molina O, Zeidouni M. Analytical approach to determine the degree of interference between multi-fractured horizontal wells. Paper SPE 185765 presented at: SPE Europec featured at 79th EAGE Conference and Exhibition; June 12-15, 2017; Paris, France.
17. Lawal H, Jackson G, Abolo N, Flores C. A novel approach to modeling and forcasting Frac hits in shale gas wells. Paper SPE 164898 presented at: the EAGE Anunual Conference & Exhibition incorporating SPE Europec; June 10-13, 2013; London, UK.
18. Thompson LG. Horizontal well fracture interference—semi-analytical modeling and rate prediction. *J Petrol Sci Eng*. 2018;160:465-473.
19. Yu W, Xu YF, Weijermars R, Wu K, Sepehrnoori K. A numerical model for simulating pressure response of well interference and well performance in tight oil reservoirs with complex-fracture geometries using the fast embedded-discrete-fracture-model method. *SPE Reserv Eval Eng*. 2018;21(2):489-502.
20. Tang HW, Yan BC, Chai Z, Zuo LH, Killough J, Sun Z. Analyzing the well-interference phenomena in the Eagle Ford Shale/Austin Chalk production system with a comprehensive compositional reservoir model. *SPE Reserv Eval Eng*. 2019;22:0827-0841.
21. Wang JL, Jia AL, Wei YS, Qi YD, Dai Y. Laplace-domain multi-well convolution for simulating pressure interference response of multiple fractured horizontal wells by use of modified Stehfest algorithm. *J Petrol Sci Eng*. 2018;161:231-247.
22. Gao DP, Liu YW, Wang DG, Han GF. Numerical analysis of transient pressure behaviors with shale gas MFHWs interference. *Energies*. 2019;12(2):262.
23. Cheng LS, Jia P, Rui ZH, Huang SJ, Xue YC. Transient responses of multifractured systems with discrete secondary fractures in unconventional reservoirs. *J Nat Gas Sci Eng*. 2017;41:49-62.
24. Zhu WY, Qi Q, Ma Q, Deng J, Yue M, Liu YZ. Unstable seepage modeling and pressure propagation of shale gas reservoirs. *Petrol Explor Dev*. 2016;43(2):261-267.
25. Bello RO, Wattenbarger RA. Multi-stage hydraulically fractured shale gas rate transient analysis. Paper SPE 126754 presented at: North Africa Technical Conference and Exhibition; February 14-17, 2010; Cairo, Egypt.
26. Ozkan E, Brown ML, Raghavan R, Kazemi H. Comparison of fractured horizontal well performance in tight sand and shale reservoirs. *SPE Reserv Eval Eng*. 2011;14(2):248-259.
27. Al-Rbeawi S. Analysis of pressure behaviors and flow regimes of naturally and hydraulically fractured unconventional gas reservoirs using multi-linear flow regimes approach. *J Nat Gas Sci Eng*. 2017;45:637-658.
28. Stalgorova E, Mattar L. Practical analytical model simulate production of horizontal wells with branch fractures. Paper SPE 162515 presented at: SPE Canadian Unconventional Resources Conference; 30 October-1 November, 2012; Calgary, AB, Canada.
29. Zhang LH, Gao J, Hu SY, Guo JJ, Liu QG. Five-region flow model for MFHWs in dual porous shale gas reservoirs. *J Nat Gas Sci Eng*. 2016;33:1316-1323.
30. Zeng J, Wang XZ, Guo JC, Zeng FH. Composite linear flow model for multi-fractured horizontal wells in heterogeneous shale reservoir. *J Nat Gas Sci Eng*. 2017;38:527-548.
31. Wang JL, Jia AL, Wei YS, Qi YD. Approximate semi-analytical modeling of transient behavior of horizontal well intercepted by multiple pressure-dependent conductivity fractures in pressure-sensitive reservoir. *J Petrol Sci Eng*. 2017;153:157-177.
32. Kim TH, Lee JH, Lee KS. Integrated reservoir flow and geomechanical model to generate type curves for pressure transient responses of a hydraulically-fractured well in shale gas reservoirs. *J Petrol Sci Eng*. 2016;146:457-472.
33. Xiao C, Yu D, Tian L, et al. A semianalytical methodology for pressure-transient analysis of multi-well-pad-prodcution scheme in shale gas reservoirs, part 1: new insight into flow regions and multi-well interference. *SPE J*. 2018;23(3):1-21.
34. Xiong X, Devegowda D, Michel Villazon GG, Sigal RF, Civan F. A fully-coupled free and adsorptive phase transport model for shale gas reservoirs including non-darcy flow effects. Paper SPE 159758 presented at: SPE Annual Technical Conference and Exhibition, October 8-10, 2012; San Antonio, TX, USA.
35. Xu BX, Haghighi M, Li XF, Cooke D. Development of new type curves for production analysis in naturally fractured shale gas/tight gas reservoirs. *J Petrol Sci Eng*. 2013;105(1):107-115.
36. Gu AH, Ding DQ, Gao ZL, Zhang AH, Tian L, Wu TP. Pressure transient analysis of multiple fractured horizontal wells in naturally fractured unconventional reservoirs based on fractal theory and fractional calculus. *Petroleum*. 2017;3(3):326-339.
37. Fan DY, Yao J, Sun H, Zeng H. Numerical simulation of multi-fractured horizontal well in shale gas reservoir considering

multiple gas transport mechanisms. *Acta Mechanica Sinica*. 2015;47(6):906-915.
38. Bonyadi M, Rahimpour MR, Esmaeilzadeh F. A new fast technique for calculation of gas condensate well productivity by using pseudo pressure method. *J Nat Gas Sci Eng*. 2012;4:35-43.
39. Al-Hussainy R, Ramey HJ. Application of real gas flow theory to well testing and deliverability forecasting. *J Pet Technol*. 1966;18:624-636.
40. Hull R, Bello H, Richmond PL, Suliman B, Portis D, Richmond P. Variable stimulated reservoir volume (SRV) simulation: eagle ford shale case study. Paper URTEC 1582061 presented at: Unconventional Resources Technology Conference; August 12-14, 2013; Denver, CO, USA.
41. Moyner O, Lie KA. The multiscale finite volume method on unstructured grids. Paper SPE 163649 presented at: SPE Reservoir Simulation Symposium; February 18-20, 2013; The Woodlands, TX, USA.
42. Civan F. Effective correlation of apparent gas permeability in tight porous media. *Transport Porous Med*. 2010;82(2):375-384.
43. Ye ZH, Chen D, Pan ZJ. A unified method to evaluate shale gas flow behaviours in different flow regions. *J Nat Gas Sci Eng*. 2015;26(C):205-215.
44. Singh H, Javadpour F, Ettehadtavakkol A, Darabi H. Nonempirical apparent permeability of shale. *SPE Reserv Eval Eng*. 2014;17(3):1-15.
45. Civan F, Rai SC, Sondergeld HC. Shale-gas permeability and diffusivity inferred by improved formulation of relevant retention and transport mechanisms. *Transport Porous Med*. 2010;86(3):925-944.

How to cite this article: Gao D, Liu Y, Pan S, Wang J, Zhou X. Longitudinal interference analysis of shale gas multi-stage fracturing horizontal wells upon high-precision pressure test. *Energy Sci Eng*. 2020;8:2387–2401. https://doi.org/10.1002/ese3.671

APPENDIX

We use finite volume method to discretize the reservoir area into nonoverlapping control volumes with a certain control volume around each center node. According to the seepage equation and boundary conditions of the multiple composite flow model given before, the partial differential equation to be solved is integrated for each control volume, and a set of discrete equations is obtained.

Fracture discrete flow equation

Based on the flow model Equation (2) of the hydraulic fractures, the volume integral equation of the control volume V is shown as follow.

$$\int_V \nabla^2 m_F \mathrm{d}V = \left(\frac{\phi_F c}{k_F}\right) \int_V \frac{\partial m_g}{\partial t} \mathrm{d}V. \tag{A1}$$

Gauss formula is used to convert the volume integral of the left diffusion term of Equation (A1) into surface integral, as shown in Equations (A2) and (A3).

$$\oint_S \nabla m_F \cdot \mathrm{d}A = \left(\frac{\phi_F c}{k_F}\right) \frac{\partial}{\partial t} \int_V m_F \mathrm{d}V, \tag{A2}$$

$$\sum_b^N (\nabla m_F \cdot A)_b = \left(\frac{\phi_F c}{k_F}\right) \frac{\partial}{\partial t} \int_V m_F \mathrm{d}V. \tag{A3}$$

Assuming that the time difference between two time steps is Δt, the distance of two adjacent grid center node is L and then the discrete equation can be converted into Equation (A4).

$$\sum_b^N \left(A \frac{m_F^a - m_F^b}{L_{a,b}}\right)_b = \frac{\phi_F c}{k_F} \frac{m_F^{n+1} - m_F^n}{\Delta t} \Delta V. \tag{A4}$$

The linearized form of Equation (A4) is:

$$\left[\left(\frac{\phi_F c \Delta V}{k_F \Delta t}\right)^{(i)} m_F^{(i+1)}\right]^{(n+1)} - \sum_b^N \left(A \frac{m_F^a - m_F^b}{L_{a,b}}\right)_b^{n+1} = \left(\frac{\phi_F c \Delta V}{k_F \Delta t} m_F\right)^n. \tag{A5}$$

On this basis, the discrete equations of stimulated reservoir volume (SRV) region and unstimulated matrix region can be further deduced.

SRV region discrete flow equation

The discrete flow equation of SRV region matrix system is shown in Equation (A6):

$$\sum_i^N \left(A \frac{m_{S,m}^a - m_{S,m}^i}{L_{a,i}}\right)_i - \alpha(m_{S,m} - m_{S,f})\Delta V = \left(\frac{\phi_{S,m} c}{k_{s,m}} + \frac{2R_g T \rho_s V_{S,L}(1-\phi_{S,m})}{k_{s,m} V_{st}(m_{S,L} + m_{S,m})^2}\right) \frac{m_{S,m}^{n+1} - m_{S,m}^n}{\Delta t} \Delta V. \tag{A6}$$

The linearized form of Equation (A6) is:

$$\left\{\left[\frac{\phi_{\mathrm{S,m}}c}{k_{\mathrm{s,m}}}+\frac{2R_{\mathrm{g}}T\rho_{\mathrm{s}}V_{\mathrm{S,L}}(1-\phi_{\mathrm{S,m}})}{k_{\mathrm{s,m}}V_{\mathrm{st}}(m_{\mathrm{S,L}}+m_{\mathrm{S,m}})^2}\right]^i\frac{\Delta V}{\Delta t}m_{\mathrm{S,m}}^{i+1}\right\}^{n+1}$$
$$-\sum_b^N\left(A\frac{m_{\mathrm{S,m}}^a-m_{\mathrm{S,m}}^b}{L_{a,b}}\right)_b^{n+1}+\alpha(m_{\mathrm{S,m}}-m_{\mathrm{S,f}})^{n+1}\Delta V \quad \text{(A7)}$$
$$=\left\{\left[\frac{\phi_{\mathrm{S,m}}c}{k_{\mathrm{s,m}}}+\frac{2R_{\mathrm{g}}T\rho_{\mathrm{s}}V_{\mathrm{S,L}}(1-\phi_{\mathrm{S,m}})}{k_{\mathrm{s,m}}V_{\mathrm{st}}(m_{\mathrm{S,L}}+m_{\mathrm{S,m}})^2}\right]\frac{\Delta V}{\Delta t}m_{\mathrm{S,m}}\right\}^n.$$

The discrete flow equation of the fracture system in SRV region is shown in Equation (A9):

$$\sum_b^n\left(A\frac{m_{\mathrm{S,f}}^a-m_{\mathrm{S,f}}^b}{L_{a,b}}\right)_b-\alpha(m_{\mathrm{S,m}}-m_{\mathrm{S,f}})\Delta V$$
$$=-\left(\frac{\phi_{\mathrm{F}}\mu_{\mathrm{g}}c_{\mathrm{g}}}{k_{\mathrm{F}}}\right)^{n+1}\frac{\left(m_{\mathrm{S,f}}^{n+1}-m_{\mathrm{S,f}}^n\right)}{\Delta t}\Delta V. \quad \text{(A8)}$$

The linearized form of Equation (A9) is:

$$\sum_b^n\left(A\frac{m_{\mathrm{S,f}}^a-m_{\mathrm{S,f}}^b}{L_{a,b}}\right)_b^{n+1}-\alpha(m_{\mathrm{S,m}}-m_{\mathrm{S,f}})^{n+1}\Delta V$$
$$+\left[\left(\frac{\phi_{\mathrm{F}}c}{k_{\mathrm{F}}}\right)^i\frac{\Delta V}{\Delta t}m_{\mathrm{S,f}}^{i+1}\right]^{n+1}=\frac{\phi_{\mathrm{F}}\mu_{\mathrm{g}}c_{\mathrm{g}}}{k_{\mathrm{F}}}\frac{\Delta V}{\Delta t}m_{\mathrm{S,f}}^n. \quad \text{(A9)}$$

Matrix region discrete flow equation

The discrete flow equation of matrix region matrix system is shown in Equation (A10):

$$\sum_b^n\left(A\frac{m_{\mathrm{M}}^a-m_{\mathrm{M}}^b}{L_{a,b}}\right)_b=-\left(\frac{\phi_{\mathrm{F}}c}{k_{\mathrm{F}}}\right)^{n+1}\frac{m_{\mathrm{M}}^{n+1}-m_{\mathrm{M}}^n}{\Delta t}\Delta V. \quad \text{(A10)}$$

The linearized form of Equation (A10) is:

$$\sum_b^n\left(A\frac{m_{\mathrm{M}}^a-m_{\mathrm{M}}^b}{L_{a,b}}\right)^{n+1}+\left[\left(\frac{\phi_{\mathrm{F}}c}{k_{\mathrm{F}}}\right)^i\frac{\Delta V}{\Delta t}m_{\mathrm{M}}^{i+1}\right]^{n+1}$$
$$=\left(\frac{\phi_{\mathrm{F}}c}{k_{\mathrm{F}}}\right)^n\frac{\Delta V}{\Delta t}m_{\mathrm{M}}^n. \quad \text{(A11)}$$

Boundary conditions discrete equations

Boundary conditions between fracture and SRV region:

$$\left(m_{\mathrm{S,f}}|_{\Gamma_3}\right)_j^{n+1}=\left(m_{\mathrm{M}}|_{\Gamma_3}\right)_j^{n+1}. \quad \text{(A12)}$$

Interface conditions between SRV region and matrix:

$$\left(m_{\mathrm{S,f}}|_{\Gamma_3}\right)_i^{n+1}=\left(m_{\mathrm{M}}|_{\Gamma_3}\right)_i^{n+1}. \quad \text{(A13)}$$